HHS Public Access

Author manuscript

IEEE Trans Med Imaging. Author manuscript; available in PMC 2019 February 01.

Published in final edited form as:

IEEE Trans Med Imaging. 2018 February ; 37(2): 536–546. doi:10.1109/TMI.2017.2764425.

Thermo-Acoustic Ultrasound for Detection of RF-Induced Device Lead Heating in MRI

Neerav Dixit [Student Member, IEEE],
Department of Electrical Engineering, Stanford University, Stanford, CA 94305 USA

Pascal P. Stang,
Department of Electrical Engineering, Stanford University, Stanford, CA 94305 USA. He is now with Procyon Engineering, San Jose, CA 95124 USA

John M. Pauly [Member, IEEE], and
Department of Electrical Engineering, Stanford University, Stanford, CA 94305 USA

Greig C. Scott [Member, IEEE]
Department of Electrical Engineering, Stanford University, Stanford, CA 94305 USA

Abstract

Patients who have implanted medical devices with long conductive leads are often restricted from receiving MRI scans due to the danger of RF-induced heating near the lead tips. Phantom studies have shown that this heating varies significantly on a case-by-case basis, indicating that many patients with implanted devices can receive clinically useful MRI scans without harm. However, the difficulty of predicting RF-induced lead tip heating prior to scanning prevents numerous implant recipients from being scanned. Here, we demonstrate that thermo-acoustic ultrasound (TAUS) has the potential to be utilized for a prescan procedure assessing the risk of RF-induced lead tip heating in MRI. A system was developed to detect TAUS signals by four different TAUS acquisition methods. We then integrated this system with an MRI scanner and detected a peak in RF power absorption near the tip of a model lead when transmitting from the scanner's body coil. We also developed and experimentally validated simulations to characterize the thermo-acoustic signal generated near lead tips. These results indicate that TAUS is a promising method for assessing RF implant safety, and with further development, a TAUS pre-scan could allow many more patients to have access to MRI scans of significant clinical value.

Index Terms

Implanted devices; Magnetic Resonance Imaging (MRI); RF heating; thermoacoustic imaging

I. Introduction

The long conductive leads of implanted medical devices such as cardiac pacemakers, implantable cardioverter/defibrillators (ICDs), and neurostimulators create a risk of tissue

heating in MRI. The transmit RF fields in MRI can induce significant currents on the leads, causing excessive heating in tissue in contact with the lead tips [1], [2]. This RF-induced heating has been observed *in vivo* and has injured patients undergoing MRI scans [3], [4]. Consequently, many implanted medical devices and leads have been contraindicated for MRI, preventing numerous implant recipients from receiving MRI scans [5]. Recently, "MRI-conditional" devices, employing modified lead structures, reduce coupling to the transmit RF fields to allow scanning under certain limitations such as reduced RF power [6]–[8]. These limitations are often too strict to allow for the acquisition of clinically useful images [9] and do not benefit legacy devices.

RF-induced tip heating in MRI depends on numerous factors, including the structure of the lead, its length relative to the RF wavelength, and its position and orientation in the RF transmit coil [10]–[14]. Electromagnetic simulations to assess RF-induced heating require detailed modeling of the lead structure, the lead path in the body, and the patient orientation relative to the RF transmit coil. An exclusion of fine details can significantly impact simulated heating levels [15], yielding a disparity with validations. In phantoms, the amount of heating is significant for certain lead configurations, yet remains below physiologically harmful levels for many others. Despite the uncertainty, many implant recipients have been scanned without issue using RF power levels well above the manufacturer-recommended limits [16], [17]. RFinduced tip heating can vary dramatically on a case-by-case basis; hence, many patients who are currently restricted from receiving MRI scans could have undergone these scans at normal RF power levels without adverse effects. However, the complexity of the many interrelated factors that affect lead tip heating makes assessing the risk of heating for each individual patient difficult. A pre-scan to reliably assess this risk on a case-by-case basis could have a significant clinical impact.

The ideal pre-scan should be done with the patient positioned in the scanner and subjected to RF coupling by the same RF transmit coil(s) used for imaging but with minimal RF energy deposition to prevent heating. Detailed modeling of the lead, the patient, and the RF transmit coil(s) should be unnecessary. A variety of RF safety pre-scans have previously been proposed. B1 mapping can quantify the RF current induced on leads from the B1 artifacts during RF transmit [18]–[21]. Alternatively, the reversal of polarization during RF transmit and/or receive exploits these B1 artifacts for the acquisition of MR images that highlight RF coupling to leads [22]. Another pre-scan technique analyzes perturbations of the RF transmit coil S-parameters to determine the degree of coupling between these channels and conductive leads [23]. Each of these methods has limitations; B1 artifact methods work best when the lead path has a simple geometry and is oriented along the B0 field direction, and induced lead currents cannot be easily quantified from S-parameter deviations.

In this work, we propose the use of thermo-acoustics to assess RF implant safety. RF power absorption in a region – expressed in terms of specific absorption rate (SAR) – can cause thermo-elastic expansion and sound emission. We demonstrate that thermo-acoustic ultrasound (TAUS) is a viable technique to detect the peaks in local SAR near lead tips that are associated with RF-induced lead tip heating in MRI.

II. Theory

A. The Thermo-Acoustic Effect

TAUS is a hybrid imaging technique that uses RF excitation and acoustic reception to detect RF power absorption [24], [25]. The basis of TAUS is the thermo-acoustic effect in which the absorption of RF energy creates acoustic waves. When RF energy is absorbed by a material, the resulting heating causes local thermal expansion, which in turn creates a pressure distribution that propagates through space as an acoustic wave. Although thermal expansion is the physical source of the thermo-acoustic signal, only a minute temperature rise is required to create a perceptible signal in tissue. A temperature increase of 1 mK can create a pressure of approximately 800 Pa, which exceeds the noise floor of typical ultrasonic transducers [26].

The thermal confinement condition for thermo-acoustics specifies that the effects of heat transfer can be neglected when the characteristic thermal diffusion and convection lengths over the duration of each RF excitation are much smaller than the desired spatial resolution [27]. When this condition is satisfied, the thermo-acoustic effect in a uniform, nonattenuating medium can be described by the wave equation

$$\left(\nabla^2 - \frac{1}{v_s^2}\frac{\partial^2}{\partial t^2}\right) p(\vec{r}, t) = -\frac{\beta}{C}\frac{\partial H(\vec{r}, t)}{\partial t}. \quad (1)$$

Here, p is the thermo-acoustic pressure, v_s is the speed of sound, β is the thermal expansion coefficient, C is the heat capacity per unit mass, and H is the RF power absorbed per unit volume or, given density ρ and the instantaneous local SAR:

$$H(\vec{r}, t) = \rho SAR(\vec{r}, t). \quad (2)$$

Assuming a narrowband RF transmit, the instantaneous local SAR can be approximated as a separable function of position and time:

$$SAR(\vec{r}, t) = G(\vec{r})P(t). \quad (3)$$

G describes the SAR spatial profile, which specifies how the SAR varies as a function of position, at the RF frequency of interest. The SAR spatial profile is determined by the electric field spatial profile and the medium's electromagnetic properties, both of which are frequency-dependent. P denotes the RF transmit power over time, which is proportional to the square of the RF transmit amplitude. Combining (1) to (3), the thermo-acoustic wave equation can be expressed as

$$\left(\nabla^2 - \frac{1}{v_s^2}\frac{\partial^2}{\partial t^2}\right) p(\vec{r}, t) = -\frac{\beta\rho}{C} G(\vec{r}) \frac{\partial P(t)}{\partial t}. \quad (4)$$

From (4), the initial pressure distribution generated by the thermo-acoustic effect following an RF impulse is determined by the SAR spatial profile G. Assuming that the properties of the medium are known, inverse methods are needed to estimate the SAR spatial profile from the signals recorded by acoustic receivers in a TAUS scan. Reflections, attenuation, and refraction of the propagating acoustic waves through a complex medium like the human body can make converting received signals to quantitative SAR values challenging. However, as in conventional ultrasound imaging, the received acoustic signals can still provide valuable information without a precise quantitative result.

By assuming an $\exp(j\omega t)$ time dependence, (4) can be transformed from the time domain to the temporal frequency domain to give

$$\left(\nabla^2 + \frac{\omega^2}{v_s^2}\right) \bar{p}(\vec{r}, \omega) = -\frac{j\omega\beta\rho}{C} G(\vec{r}) \bar{P}(\omega) \quad (5)$$

where $\bar{p}$ and $\bar{P}$ represent the thermo-acoustic pressure p and RF transmit power P in the temporal frequency domain. The linear relationship between the frequency-domain spectra of the thermo-acoustic pressure and the RF transmit power in (5) implies that thermo-acoustic signals can be generated at ultrasound frequencies by modulating the RF transmit power at these frequencies. Whereas the RF carrier frequency impacts the SAR spatial profile, the envelope of the RF transmit signal determines which acoustic frequencies are excited.

B. TAUS Acquisition Methods

Multiple modulation techniques employing pulsed and continuous wave (CW) approaches can be used for TAUS acquisition. Pulsed TAUS, as in conventional ultrasound, uses the time delay between the transmitted pulse and received signal to determine range. Because pulsed TAUS is a time-domain method, the spatial resolution is limited by the pulse duration according to the stress confinement condition – namely, the limit of the achievable resolution is the product of the pulse duration and the speed of sound [27].

Frequency-modulated continuous-wave (FMCW) acquisition methods, which are common in radar, can also be used for TAUS [28], [29]. In FMCW TAUS, the RF signal is amplitude modulated by a linear frequency modulation (LFM) chirp signal, exciting thermo-acoustic signals at frequencies within the chirp's spectrum. FMCW amplitude modulation encodes depth via frequency rather than time, allowing RF excitation and acoustic signal reception to occur simultaneously. For frequency-domain techniques, the spatial resolution is limited by

the acquisition bandwidth. The received signal is demodulated by a reverse chirp acting as a matched filter to recover SNR and resolution.

A hybrid of square-wave pulsed transmit with CW modulation can simplify drive electronics. For this square-wave modulation, an RF carrier is on/off keyed (OOK) by a square wave whose instantaneous frequency is determined by the frequency of an LFM chirp signal [30]. For an LFM square wave of 50% duty cycle and increasing frequency (hence decreasing length), Fourier analysis yields similar thermo-acoustic excitation to direct FMCW amplitude modulation, despite the transmit signal now being a pulse train. Depth encoding and demodulation are identical to other FMCW methods. Another variant of the square-wave modulation uses a square wave of fixed length but with an LFM repetition rate. This results in each RF pulse exciting the same initial thermo-acoustic pressure distribution.

Due to the frequency-domain depth encoding, CW and square-wave modulations allow for simultaneous transmit and receive, whereas a significant delay is required between transmit pulses for time-domain pulsed TAUS. For v_s = 1500 m/s, receiving unaliased signals from a 15 cm depth requires a delay of 100 μs. For 500 ns pulses, this implies a maximum duty cycle of 0.5%. Therefore, for a given duration of RF transmit, the scan time is significantly shorter for the CW and square wave methods than for pulsed modulation.

C. Maximizing TAUS SNR Under a Fixed Energy Constraint

When the thermal confinement condition is satisfied, tissue heating due to the RF excitation in TAUS is proportional to the quantity of RF energy delivered. For a pre-scan to assess RF implant safety, thermo-acoustic signals originating from the SAR peaks near lead tips must be received with sufficient SNR to ensure detection, while minimal RF energy should be delivered to prevent significant tissue heating.

The RF transmit and acoustic receive signals in TAUS have a nonlinear relationship, as the acoustic signal power is proportional to the square of the RF signal power. Although the SNR depends on multiple factors including the RF excitation mechanism, the acoustic receiver setup, and the material properties throughout the medium, this quadratic relationship implies that when transmitting a fixed quantity of RF energy, SNR always improves as the transmit power is increased. Specifically, increasing the transmit power and decreasing the transmit duration by a factor of N improves SNR by a factor of $\sqrt{N}$ while depositing the same amount of energy and therefore causing the same level of tissue heating [29].

A shorter RF excitation is possible with the time-domain pulsed method than with frequency-domain methods such as FMCW amplitude modulation and square-wave modulation, suggesting that the pulsed method may be able to use a higher transmit power level than these other methods under a fixed energy constraint and therefore achieve a better SNR. However, the RF transmit power cannot be increased to arbitrarily high levels and is limited by the peak output power of the RF power amplifier used in the transmit chain. This power limitation determines either the minimum duration of the transmit waveform or the number of repeated acquisitions using a given transmit waveform that is needed to transmit the desired quantity of RF energy. When a sufficiently large number of repeated pulsed

acquisitions is required, frequency-domain methods become viable alternatives to the pulsed method. Regardless of which acquisition method, excitation source, and receiver setup are used, RF transmit should be done using the maximum possible transmit power to maximize SNR for a given level of tissue heating.

D. Effect of SAR Spatial Profile on TAUS Signal

Using the Green's function for the wave equation in (5) and separating the spectrum of the RF transmit power from the other terms in the resulting expression, we can directly express the frequency-domain thermo-acoustic pressure as

$$\bar{p}(\vec{r},\omega) = S(\vec{r},\omega)\bar{P}(\omega) \quad (6)$$

$$S(\vec{r},\omega) = \frac{j\omega\beta\rho}{4\pi C}\iiint \frac{G(\vec{r}\,')\exp\left(j\frac{\omega}{v_s}\mid \vec{r}-\vec{r}\,'\mid\right)}{\mid \vec{r}-\vec{r}\,'\mid} d\vec{r}\,'. \quad (7)$$

S represents the spatial profiles of thermo-acoustic signals of different acoustic frequencies, which describe how the magnitude and phase of these signals vary with position.

The volumetric integral in (7) expresses how the SAR spatial profile and the acoustic wavelength affect the thermo-acoustic spatial profile. Conceptually, in TAUS the SAR spatial profile can be treated as a continuous set of acoustic point sources that generate spherical waves of varying magnitudes. Therefore, the amplitude of a thermo-acoustic wave at a given position is inversely proportional to the distance between the wave's source and the position. Additionally, the ratio between this distance and the acoustic wavelength determines the phase shift incurred by the propagating thermo-acoustic wave at that position. The varying phase shifts from the different acoustic point sources represented by the SAR spatial profile create interference patterns that strongly influence how the signal varies as a function of position. Although the specific analysis shown here applies to a uniform, non-attenuating medium, the signal's dependence on the SAR spatial profile also holds true when considering more complex scenarios.

The SAR spatial profile differs when scanning different objects, meaning that the spatial profile of the thermo-acoustic signal as a function of acoustic frequency differs as well. This makes the choice of acoustic acquisition bandwidth for each TAUS scan important, as it affects the observed signal differently on a case-by-case basis.

III. Methods

To evaluate the utility of TAUS in assessing RF implant safety in MRI, we implemented a system to obtain thermo-acoustic signals from lead tips using a variety of modulation methods. We then compared the SNRs of these methods in the case of equal transmit power and transmit duration [30]. The TAUS acquisition system was integrated with an MRI

scanner to observe the thermo-acoustic signal created by the coupling between the RF fields transmitted by the scanner's body coil and a model device lead [30]. To gain further insight into the excited thermo-acoustic signal, we developed and experimentally validated simulations of the signal generated by RF power absorption near lead tips.

A. TAUS Experimental Setup

Fig. 1 shows the setup used to induce and detect thermo-acoustic signals outside of the MRI scanner. A Medusa MRI console [31] and a series of custom electronics generated the desired transmit waveforms, each using a 64 MHz RF carrier to emulate the RF frequency used in a 1.5 T MRI scanner. The RF transmit signal was amplified by a 200 W power amplifier (AR Kalmus model LA200HP-CE 0.5–100 MHz), high-pass filtered to reduce undesirable harmonics, passed through a bandpass circulator to protect the power amplifier from reflections, and then used to directly drive a stripped coaxial cable immersed in saline solution. An Olympus V303-SU 1 MHz immersion ultrasonic transducer received the thermo-acoustic signal that was generated near the exposed conductor at the coaxial cable tip. The transducer signal was notch filtered to attenuate any feedthrough of the transmit signal, amplified by an AD797 op amp with a 40 dB gain, and low-pass filtered before reaching the Medusa RF receive port. The received signal was then digitized by the Medusa ADC, digitally demodulated, and sent through a USB connection to a computer for post-processing. Using the Medusa console for transmit and receive allowed for coherent post-processing of the received signal.

B. Comparison of TAUS Acquisition Methods

Four different TAUS acquisition methods were used. To implement each method, we built a transmit chain to generate the desired RF transmit waveform, as detailed in Appendix A[1]. The transmit waveforms were characterized at the output of the RF power amplifier using the setup in Fig. 2a.

For pulsed TAUS (Fig. 2b), a 500 ns pulse of the 64 MHz carrier was sent to the power amplifier. For FMCW amplitude modulation (Fig. 2c), a 2 ms LFM chirp with a 1 MHz center frequency and a 375 kHz bandwidth was used to amplitude modulate the 64 MHz carrier. Two variants of square-wave modulation were tested as well. In both cases, a 2 ms LFM chirp with a 1 MHz center frequency and a 375 kHz bandwidth determined the repetition frequency of the square wave used for OOK modulation of the 64 MHz carrier. In the first case, a square wave with a 50% duty cycle was used, whereas the second variant passed the 64 MHz carrier to the amplifier for 500 ns during each period of the square wave.

To compare these four TAUS acquisition methods, each drove the experimental setup in Fig. 1 at the same transmit power level for a total duration of 4 ms, ensuring the same total RF energy deposition for each method. For the pulsed TAUS method, 8000 acquisitions using 500 ns pulses were averaged, and for the FMCW and square-wave modulation methods, two 2 ms acquisitions were averaged.

[1]Appendix A is available in the supplementary files / multimedia tab.

C. TAUS for Lead Tip SAR in an MRI Setting

We also interfaced our TAUS system with a GE Signa Excite 1.5 T scanner using the setup diagrammed in Fig. 3. The scanner's 16 kW body coil amplifier (Analogic AN8103-CP) was instead driven by the transmit chains used in the TAUS system to produce the desired RF waveforms in the body coil. The Medusa console was configured in slave mode so that it would only transmit when triggered by the transmit gate associated with the body coil. This ensured synchronization between the TAUS RF transmit and the scanner electronics. The RF waveforms transmitted by the body coil were characterized by placing a pickup loop in the scanner bore.

A model lead, consisting of an insulated wire with 7 mm of insulation stripped at one end, was placed in the scanner bore to demonstrate TAUS detection of RF-induced lead tip heating in an MRI setting. The end of the model lead with the exposed conductor was immersed in a tub of saline solution, and the other end of the lead remained floating without any electrical connections. An Olympus V303-SU 1 MHz immersion ultrasonic transducer in the saline solution captured the thermo-acoustic signal generated near the lead tip. An OPA847-based preamplifier and an OPA842-based LED driver were powered by a 9 V non-magnetic battery and placed in an RF-shielded box attached to the transducer. The LED output from the shielded box was optically coupled to a photo-receiver outside of the scan room to prevent electromagnetic interference in the scanner bore from distorting the received signal. After low-pass filtering to attenuate any transmit feedthrough, the signal reached the Medusa's RF receive port.

To excite a thermo-acoustic signal at the model lead tip in the scanner bore, we used an FMCW amplitude-modulated transmit to the body coil. Each LFM chirp was 3 ms in duration, had a 1 MHz center frequency, and spanned a 375 kHz bandwidth. For each TAUS scan, 250 acquisitions were averaged. To perform the scans, a dummy MRI sequence with a TR of approximately 500 ms was initiated in the scanner console to trigger one TAUS acquisition per TR. Although the absolute transmit power levels were not measured, multiple scans of the same duration were done using a range of transmit power levels to observe how SNR varied with the relative transmit power.

D. TAUS Simulation

The thermo-acoustic signal is determined by the acoustic frequencies excited by the RF transmit modulation and the signal's spatial profiles for these excited frequencies, which depend on the medium and the SAR spatial profile. When evaluating SAR near device lead tips, a common assumption is that for a particular lead structure, the shape of the SAR spatial profile at a given RF frequency does not depend on the incident RF field pattern along the lead [32]. Therefore, the SAR spatial profile is identical up to a scale factor for any incident field profile. This implies that for a given RF excitation near the RF frequency of interest, the thermo-acoustic signal propagating from the lead tip will be identical up to a scale factor for any incident field profile as well. We developed a simulation procedure to characterize how the spatial profile of this scaled thermo-acoustic signal from a given lead varies with acoustic frequency without prior knowledge of the incident fields generated by the RF transmit coil(s). Finite-difference time-domain (FDTD) simulations were performed

for two model leads, each with a wire diameter of 2.04 mm and an insulation outer diameter of 3.10 mm. One model lead had 7 mm of insulation stripped at one end, whereas the other had 14 mm of stripped insulation (Fig. 4a).

Each simulation was conducted with two distinct steps, an electromagnetic simulation followed by an acoustic simulation [33]. The electromagnetic simulation, performed using Sim4Life (Zurich MedTech, Zurich, Switzerland), first determined the spatial profile of the local SAR near the lead tip up to a scale factor. The lead was modeled as immersed in a uniform conductive medium, and a 64 MHz plane wave source was placed at an arbitrary position along the lead to generate electric fields oriented tangentially to the lead path (Fig. 4b). The simulated SAR spatial profile served as the pressure source distribution for the acoustic simulation that characterized the shape of the thermo-acoustic signal's spatial profile at a range of acoustic frequencies. For the acoustic simulation, we created a Matlab (Mathworks, Natick, MA, USA) script to perform an FDTD simulation of (4) for a given SAR spatial profile in 2D cylindrical coordinates with azimuthal symmetry, as described in Appendix B[2] [34], [35].

To ensure that the FDTD simulation results were replicable and not significantly influenced by the choices of simulation parameters, simulations were also performed using the finite-element simulation software COMSOL Multiphysics (COMSOL, Inc., Burlington, MA, USA), as discussed in Appendix C[3]. The results of these two simulation methods were compared qualitatively to ensure that they were consistent.

The results of the thermo-acoustic simulations were used to estimate the relative signal intensities observed by a transducer positioned at different points in a plane. Fig. 5b shows the orientation of these measurement planes, which are each defined by a constant value of x in the displayed coordinate system. To determine the relative transducer signal at a given position, the size and shape of the desired transducer surface were specified, and the frequency-domain simulation results were summed over the grid points covered by this surface. Then, the resulting magnitude data within the desired excitation bandwidth was summed to determine the relative signal level. The signal profile in each measurement plane was also estimated without summing over the transducer surface to determine the effect of the transducer size and shape on the observed signal profile.

E. Experimental Validation of TAUS Simulation

To validate the simulations, the setup shown in Fig. 5 was used to determine how the observed thermo-acoustic signal varies with transducer positioning for two different leads at two different acoustic frequency ranges. TAUS measurements of both leads in Fig. 4a were taken at a series of transducer positions in a 2D plane (Fig. 5b) by attaching a transducer to the stage of a 2D CNC plotter (Makeblock XY Plotter). The transducer was moved at 1 mm increments across both dimensions of each measurement plane to perform acquisitions in a 15 mm by 15 mm area. At each position 250 FMCW acquisitions of 375 kHz bandwidth, 4 ms duration, and a center frequency of either 0.5 MHz or 1 MHz were averaged, and an 8 ms

[2]Appendix B is available in the supplementary files / multimedia tab.
[3]Appendix C is available in the supplementary files / multimedia tab.

period between the start of each acquisition resulted in a scan duration of 2 s per point. To excite thermo-acoustic signals, a 200 W RF power amplifier (AR Kalmus model LA200HP-CE 0.5–100 MHz) directly drove a resonant toroid [36] that was coupled to the model leads. Olympus V318-SU (0.5MHz) and V303-SU (1 MHz) transducers were used for ultrasound reception for the 0.5 MHz and 1 MHz acquisitions.

IV. Results

A. Comparison of TAUS Acquisition Methods

The transmit waveforms generated for each TAUS acquisition method, shown in Fig. 2b–e, were slightly altered from their idealized forms due to the power amplifier's asymmetric rise and fall times. Fig. 6 shows the thermo-acoustic SNR versus range for each acquisition method that drove the setup in Fig. 1. Here, the lead tip was positioned 6 cm from the transducer. The significant signal at 0 distance from the transducer is a result of direct feedthrough of the transmit signal to the receive chain. Using the stripped coaxial cable source and a 1 MHz transducer, the SNRs of the pulsed and FMCW amplitude modulation methods at the signal source were very similar, whereas the square-wave modulation methods had somewhat lower SNRs.

B. Demonstration of TAUS in an MRI Scanner

The setup used to generate TAUS transmit waveforms in the MRI scanner's body coil is not specific to the scanner used in the experiment; only access to the body coil amplifier and a transmit gate associated with the body coil were required. Conceptually, a TAUS modulation system could augment any MRI scanner through an RF routing switch to the transmit coil.

When transmitting to the high-Q MRI body coil, the RF envelopes for the pulsed and square-wave modulation methods were significantly altered, with large rise and fall times (Fig. 3b). This reduces SNR efficiency and damages the spatial resolution of the pulsed method, for which resolution expands linearly with pulse length. These coils also affect the FMCW amplitude-modulated transmit by filtering the AM sidebands, reducing the amount of modulation in the transmit signal and decreasing thermo-acoustic excitation at the desired acoustic frequencies (Fig. 3c). Overall, the effects of filtering were less deleterious for the FMCW amplitude-modulated waveform than for the pulsed waveform. Considering SNR, scan time, and the effects of filtering, FMCW amplitude modulation was deemed to be the most suitable TAUS acquisition method for an MRI setting.

The ultrasonic transducer used to conduct measurements in the scanner bore was not designed to be MRI-compatible, and it may have contained ferromagnetic materials or a ferrous impedance-matching inductor, as a 12 dB reduction in transducer sensitivity was measured when in the scanner's 1.5 T field. Despite this loss in sensitivity, a significant thermo-acoustic signal was detected from the lead tip as a result of coupling between the RF fields from the body coil transmit and the model lead placed in the scanner bore (Fig. 7). The SNR was roughly proportional to the transmit power, as expected from TAUS physics, and an SNR of 122 was achieved at the highest transmit power level when averaging 250 acquisitions, each using a 3 ms FMCW amplitude-modulated excitation.

C. TAUS Simulation Results and Validation

Fig. 4c shows the shape of the SAR spatial profiles at 64 MHz from the FDTD electromagnetic simulations of both leads. For both leads, the SAR is highest along the exposed conductor, with peaks near the start and end of the conductor. This SAR distribution matches simulation results from other work [32]. Results of the acoustic simulations are displayed in Fig. 4d, which shows the scaled spatial profiles of the thermo-acoustic signal magnitudes for both leads at acoustic frequencies of 0.5 MHz and 1 MHz. The differences in the SAR spatial profiles between the two simulated leads result in different spatial profiles for the thermo-acoustic signals propagating from the leads. For each lead, the signal magnitude varies more rapidly in space for the 1 MHz acoustic frequency due to the shorter acoustic wavelength as compared to the 0.5 MHz acoustic frequency.

Simulated thermo-acoustic signals from both leads are shown in 2D measurement planes in Fig. 8. These FDTD simulations used 375 kHz bandwidths and center frequencies of 0.5 MHz and 1 MHz for the TAUS acquisition parameters. The simulated magnitude signals observed by finite-sized transducers positioned at different points in a measurement plane are shown along with the experimentally measured transducer signals from the validation experiment in Fig. 9. The measured and simulated signal profiles in Fig. 9 appear very similar for both leads and for both acquisition center frequencies within the measured field of view, demonstrating that the simulations accurately characterize thermo-acoustic signals from lead tips.

V. Discussion

A. Filtering in the TAUS System to Reduce Interference

When assembling our TAUS system, the importance of minimizing both nonlinearities in the system and feedthrough from the transmit chain to the receive chain became very apparent. Nonlinear distortion in the transmit chain can add the second harmonic of the modulated RF signal to the transmit signal, effectively demodulating the desired thermo-acoustic signal in the transmit chain. Direct feedthrough to the receive chain or coupling to the transducer electronics of this demodulated signal creates artifacts in the received signal. Feedthrough of the undistorted RF transmit followed by nonlinear distortion of the resulting RF signal in the receive chain also creates these artifacts. A large feedthrough signal can also saturate the receive electronics, preventing detection of the desired thermo-acoustic signal. As diagrammed in Figs. 1 and 5, we included a series of filters in the TAUS system to reduce these undesirable effects. When detecting thermo-acoustic signals in the MRI scanner bore, the system was especially sensitive to direct RF feedthrough, so fiber optic coupling of the receive signal to a photo-receiver outside the scanner was used to preserve the signal integrity.

B. Detection SNR versus Heating During TAUS Pre-Scan

The experiment in the MRI scanner achieved thermo-acoustic signal detection with an SNR of 122 when taking 250 averages of 3 ms FMCW acquisitions. This indicates that a single 3 ms excitation would achieve an SNR of approximately 7.7. Although the absolute transmit power level in the experiment was not measured, the 16 kW rating of the RF amplifier along

with the sinusoidal modulation of the transmit waveform indicate that the average transmit power did not exceed 8 kW. Neglecting thermal diffusion and perfusion and assuming a heat capacity of 3660 J/(kg°C) in tissue, inducing a 1°C temperature increase in 1 g of tissue with a 3 ms transmit signal requires an average power of 1.22 kW to be coupled to the lead tip. Even assuming that the upper bound of 8 kW was transmitted, a very large percentage – over 15% – of the transmit power would need to be coupled directly to the lead tip to cause a temperature increase of 1°C in 1 g, which is still below established safety standards. This degree of coupling is highly unlikely, indicating that our experimental setup could safely attain an SNR of 7.7.

Additionally, significant SNR gains should be achievable over this proof-of-concept demonstration. Using MRIcompatible transducers would prevent the significant loss in transducer sensitivity observed in the scanner's magnetic field. Adding more ultrasonic receive elements or using a transducer array would further improve the SNR, as would performing the acquisition at the acoustic bandwidth best matched to the lead's SAR spatial profile.

The presence of a strong thermo-acoustic signal from a lead tip in an MRI setting demonstrates that TAUS is a viable method to safely detect the SAR peaks associated with RF-induced heating at lead tips.

C. Transducer Size Affects Sensitivity to Receiver Positioning

The simulated and measured transducer signals in Fig. 9 vary much more rapidly in space than the simulated signal magnitudes in Fig. 8. This indicates that summing of the thermo-acoustic signal over the transducer surface has a significant impact on the signal's spatial profile. The variation in signal phase displayed in Fig. 8 explains this effect. When the center of the transducer is positioned near the signal peak, the signal phase is relatively uniform throughout the circular transducer surface, resulting in constructive interference of the thermo-acoustic signal over the surface. As the transducer moves away from the peak, the transducer diameter becomes large relative to the rate of phase variation, and destructive interference decreases the total signal magnitude. This result shows that the acoustic receiver size can significantly impact the dependence of the observed signal on receiver positioning.

D. Simulations for Development of Robust TAUS Pre-Scan

Our simulations of the thermo-acoustic signal were validated for multiple leads and TAUS acquisition frequencies, suggesting that these simulations can accurately characterize thermo-acoustic signals at different acoustic frequencies for a variety of lead structures. Although the simulation procedure used here applies to cylindrical leads immersed in a uniform medium, it can be generalized to arbitrary lead geometries and nonuniform media by using a full 3D simulation geometry.

We can use these simulations to evaluate how the observed thermo-acoustic signal varies with the lead structure, transducer size, and acquisition bandwidth. Characterizing the signal's dependence on these factors can provide insight into how best to design a robust TAUS system that can consistently identify dangerous SAR peaks at lead tips with high sensitivity and specificity. For example, the impact of acoustic receiver size indicated by the

differences between the magnitude signal maps (Fig. 8) and the transducer signal maps (Fig. 9) has key implications for the development of an accurate prescan. A robust system should not be very sensitive to the positioning of the acoustic receivers relative to the lead tip; otherwise, seemingly minor setup imprecisions could lead to incorrect safety assessments from the TAUS pre-scan. Using a phased array transducer could help reduce this sensitivity by allowing for electronic focusing to the known lead tip location. The simulations can also help determine a suitable acquisition bandwidth for the TAUS pre-scan by illustrating how thermo-acoustic signals from different types of leads vary with acoustic frequency.

E. TAUS for SAR Mapping

As the SAR spatial profile determines the thermo-acoustic pressure source distribution, a TAUS pre-scan could theoretically be used to perform SAR mapping for MRI [37]. Generating a SAR map using TAUS would require solving an inverse problem using pressure data obtained from acoustic receivers positioned around the volume of interest. However, positioning transducers around a patient in an MRI scanner and ensuring that these transducers are both acoustically coupled to the body and have a sufficient acoustic window to the volume of interest would be challenging. Additionally, obtaining accurate SAR values from this inverse problem may be difficult due to the complexities of reflection, refraction, and attenuation as acoustic waves propagate through the body. Very high bandwidth receivers would also be required to characterize both areas with slow-varying SAR spatial profiles and those with fast-varying distributions due to the differences in the thermo-acoustic signal as a function of acoustic frequency for different SAR distributions.

F. Performing a TAUS Pre-Scan for Lead Tip Heating

Rather than solving an image reconstruction problem, a TAUS pre-scan to assess the risk of lead tip heating would only need to detect the presence of a large, spatially sparse thermo-acoustic signal. The implementation of this pre-scan would involve a multi-step protocol to ensure accurate characterization of the lead tip SAR. Electromagnetic modeling of implant leads can determine the shape of the SAR distribution at the lead tip, allowing simulations to estimate how the thermo-acoustic signal varies with the acquisition bandwidth and the SAR magnitude. In this case of a known SAR spatial pattern, these simulations may allow for a more reliable estimate of quantitative SAR values from TAUS due to the greater certainty regarding the spatial profile of the generated thermo-acoustic signal. Using knowledge of the lead tip position, an ultrasonic transducer array can then be appropriately positioned to facilitate a robust pre-scan, and a “red-flag” signal level can be set to indicate a threshold beyond which the risk of lead tip heating is deemed excessive. Finally, the pre-scan will be performed with the patient positioned in the scanner, and the resulting signal level can be compared to the “red-flag” threshold to determine whether the proposed MRI scan is safe or unsafe to perform.

VI. Conclusion

The inability to determine the risk of RF-induced heating near the lead tips of implanted medical devices currently restricts many patients from receiving clinically important MRI scans. We have assembled a TAUS system, compared several acquisition methods, and

demonstrated that our system can augment an MRI scanner to detect the SAR peaks that cause RF-induced heating at lead tips. Simulations of the TAUS signal originating from lead tips were also developed and experimentally validated, providing insight into how the SAR spatial profile near lead tips affects propagation of the thermo-acoustic signal at a range of acoustic frequencies. Using this simulation procedure, the effects of different parameters on a TAUS system can be better understood. With further development of the TAUS system, a TAUS pre-scan may allow for an assessment of the dangers of RF-induced lead tip heating in MRI on a case-by-case basis.

Supplementary Material

Refer to Web version on PubMed Central for supplementary material.

Acknowledgments

This work was supported in part by the NIH under grants R01EB008108 and P01CA159992, in part by the DARPA MEDS program, in part by the Department of Defense (DoD) through the National Defense Science & Engineering Graduate Fellowship (NDSEG) program, and in part by the Stanford Graduate Fellowship program.

References

1. Nitz W, Oppelt A, Renz W, Manke C, Lenhart M, Link J. On the heating of linear conductive structures as guide wires and catheters in interventional MRI. J Magn Reson Imaging. Jan; 2001 13(1):105–114. [PubMed: 11169811]
2. Nyenhuis J, Park S, Kamondetdacha R, Amjad A, Shellock F, Rezai A. MRI and implanted medical devices: basic interactions with an emphasis on heating. IEEE Trans Device Mater Rel. Sep; 2005 5(3):467–480.
3. Spiegel J, Fuss G, Backens M, Reith W, Magnus T, Becker G, Moringlane JR, Dillmann U. Transient dystonia following magnetic resonance imaging in a patient with deep brain stimulation electrodes for the treatment of Parkinson disease: Case report. J Neurosurg. Oct; 2003 99(4):772–774. [PubMed: 14567615]
4. Henderson JM, Tkach J, Phillips M, Baker K, Shellock FG, Rezai AR. Permanent neurological deficit related to magnetic resonance imaging in a patient with implanted deep brain stimulation electrodes for Parkinson's disease: Case report. Neurosurgery. Nov.2005 57(5):E1063. [PubMed: 16284543]
5. Kalin R, Stanton MS. Current clinical issues for MRI scanning of pacemaker and defibrillator patients. Pacing Clin Electrophysiol. Apr; 2005 28(4):326–328. [PubMed: 15826268]
6. Ahmed FZ, Morris GM, Allen S, Khattar R, Mamas M, Zaidi A. Not all pacemakers are created equal: MRI conditional pacemaker and lead technology. J Cardiovasc Electrophysiol. Sep; 2013 24(9):1059–1065. [PubMed: 24016320]
7. Ferreira AM, Costa F, Tralhão A, Marques H, Cardim N, Adragão P. MRI-conditional pacemakers: current perspectives. Med Devices (Auckl). May.2014 7:115–124. [PubMed: 24851058]
8. Shinbane JS, Colletti PM, Shellock FG. Magnetic resonance imaging in patients with cardiac pacemakers: era of "MR conditional" designs. J Cardiovasc Magn Reson. Oct.2011 13:63. [PubMed: 22032338]
9. Larson P, Richardson R, Starr P, Martin A. Magnetic resonance imaging of implanted deep brain stimulators: Experience in a large series. Stereot Funct Neuros. Mar; 2008 86(2):92–100.
10. Zikria J, Machnicki S, Rhim E, Bhatti T, Graham R. MRI of patients with cardiac pacemakers: A review of the medical literature. Am J Roentgenol. Feb; 2011 196(2):390–401. [PubMed: 21257892]
11. Nordbeck P, Weiss I, Ehses P, Ritter O, Warmuth M, Fidler F, Herold V, Jakob P, Ladd M, Quick H, Bauer W. Measuring RF-induced currents inside implants: Impact of device configuration on MRI

safety of cardiac pacemaker leads. Magn Reson Med. Mar; 2009 61(3):570–578. [PubMed: 19132759]

12. Armenean C, Perrin E, Armenean M, Beuf O, Pilleul F, Hervé S. RF-induced temperature elevation along metallic wires in clinical magnetic resonance imaging: influence of diameter and length. Magn Reson Med. Nov; 2004 52(5):1200–1206. [PubMed: 15508156]
13. Rezai AR, Finelli D, Nyenhuis JA, Hrdlicka G, Tkach J, Sharan A, Rugieri P, Stypulkowski PH, Shellock FG. Neurostimulation systems for deep brain stimulation: in vitro evaluation of magnetic resonance imaging-related heating at 1.5 Tesla. J Magn Reson Imaging. Mar; 2002 15(3):241–250. [PubMed: 11891968]
14. Baker KB, Tkach JA, Phillips MD, Rezai AR. Variability in RF-induced heating of a deep brain stimulation implant across MR systems. J Magn Reson Imaging. Dec; 2006 24(6):1236–1242. [PubMed: 17078088]
15. Guerin, B., Serano, P., Iacono, MI., Herrington, T., Widge, A., Dougherty, D., Bonmassar, G., Angelone, LM., Wald, L. Patient specific modeling of deep brain stimulation patients for MRI safety studies. Proc. 25th Ann. Meeting ISMRM; 2017. p. 12
16. Martin ET, Coman JA, Shellock FG, Pulling CC, Fair R, Jenkins K. Magnetic resonance imaging and cardiac pacemaker safety at 1.5-Tesla. J Am Coll Cardiol. Apr; 2004 43(7):1315–1324. [PubMed: 15063447]
17. Mollerus M, Albin G, Lipinski M, Lucca J. Magnetic resonance imaging of pacemakers and implantable cardioverter-defibrillators without specific absorption rate restrictions. Europace. Jul; 2010 12(7):947–951. [PubMed: 20353963]
18. Bosch M, Moerland M, Lagendijk J, Bartels L, Berg C. New method to monitor RF safety in MRI-guided interventions based on RF induced image artefacts. Med Phys. Feb; 2010 37(2):814–821. [PubMed: 20229891]
19. Griffin G, Anderson K, Celik H, Wright G. Safely assessing radiofrequency heating potential of conductive devices using imagebased current measurements. Magn Reson Med. Jan; 2015 73(1): 427–441. [PubMed: 24452789]
20. Venook, RD., Overall, WR., Shultz, K., Conolly, S., Pauly, JM., Scott, GC. Monitoring induced currents on long conductive structures during MRI. Proc. 16th Ann. Meeting ISMRM; 2008. p. 898
21. Etezadi-Amoli M, Stang P, Kerr A, Pauly J, Scott G. Controlling radiofrequency-induced currents in guidewires using parallel transmit. Magn Reson Med. Dec; 2015 74(6):1790–1802. [PubMed: 25521751]
22. Overall W, Pauly J, Stang P, Scott G. Ensuring safety of implanted devices under MRI using reversed RF polarization. Magn Reson Med. Sep; 2010 64(3):823–833. [PubMed: 20593374]
23. Ellenor C, Stang P, Etezadi-Amoli M, Pauly J, Scott G. Offline impedance measurements for detection and mitigation of dangerous implant interactions: An RF safety prescreen. Magn Reson Med. Mar; 2015 73(3):1328–1339. [PubMed: 24623586]
24. Kruger R, Kopecky K, Aisen A, Reinecke D, Kruger G, Kiser W. Thermoacoustic CT with radio waves: a medical imaging paradigm. Radiology. Apr; 1999 211(1):275–278. [PubMed: 10189483]
25. Kruger R, Reinecke D, Kruger G. Thermoacoustic computed tomography–technical considerations. Med Phys. Sep; 1999 26(9):1832–1837. [PubMed: 10505871]
26. Wang LV, Hu S. Photoacoustic tomography: in vivo imaging from organelles to organs. Science. Mar; 2012 335(6075):1458–1462. [PubMed: 22442475]
27. Xu M, Wang L. Photoacoustic imaging in biomedicine. Rev Sci Instrum. Apr.2006 77(4):041101.
28. Scott, G., Etezadi-Amoli, M., Stang, P., Nan, H., Aliroteh, M., Arbabian, A., Pauly, J. Thermo-acoustic ultrasound detection of RF coil and tip SAR. Proc. 23th Ann. Meeting ISMRM; 2015. p. 377
29. Nan H, Arbabian A. Peak-power-limited frequency-domain microwave-induced thermoacoustic imaging for handheld diagnostic and screening tools. IEEE Trans Microw Theory Techn. Jul; 2017 65(7):2607–2616.
30. Dixit, N., Stang, P., Pauly, J., Scott, G. Thermo-acoustic ultrasound detection of RF tip heating in MRI. Proc. 24th Ann. Meeting ISMRM; 2016. p. 349

31. Stang PP, Conolly SM, Santos JM, Pauly JM, Scott GC. Medusa: a scalable MR console using USB. IEEE Trans Med Imaging. Feb; 2012 31(2):370–379. [PubMed: 21954200]

32. Park S, Kamondetdacha R, Nyenhuis J. Calculation of MRI-induced heating of an implanted medical lead wire with an electric field transfer function. J Magn Reson Imaging. Nov; 2007 26(5):1278–1285. [PubMed: 17969143]

33. Dixit, N., Stang, P., Pauly, J., Scott, G. FDTD simulation of thermoacoustic ultrasound for detection of RF tip heating. Proc. 25th Ann. Meeting ISMRM; 2017. p. 483

34. Diebold GJ, Sun T. Properties of photoacoustic waves in one, two, and three dimensions. Acustica. Jul; 1994 80(4):339–351.

35. Inan, US., Marshall, RA. Numerical electromagnetics: the FDTD method. Cambridge, UK: Cambridge University Press; 2011. p. 168-169.sec 7.5

36. Etezadi-Amoli M, Stang P, Kerr A, Pauly J, Scott G. Interventional device visualization with toroidal transceiver and optically coupled current sensor for radiofrequency safety monitoring. Magn Reson Med. Mar; 2015 73(3):1315–1327. [PubMed: 24691876]

37. Winkler S, Picot P, Thornton M, Rutt B. Direct SAR mapping by thermoacoustic imaging: A feasibility study. Magn Reson Med. Oct; 2017 78(4):1599–1606. [PubMed: 27779779]

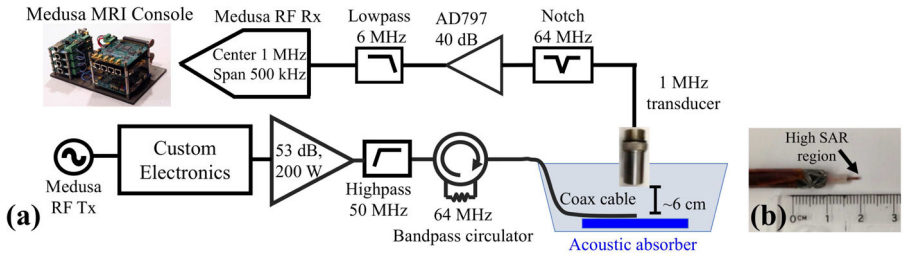

Fig. 1.

(a) Transmit and receive chain of the setup used to compare different TAUS acquisition methods. For the various methods, different electronics were used in “Custom Electronics” block, and the Medusa console was programmed differently. (b) End of the stripped coaxial cable used as the signal source.

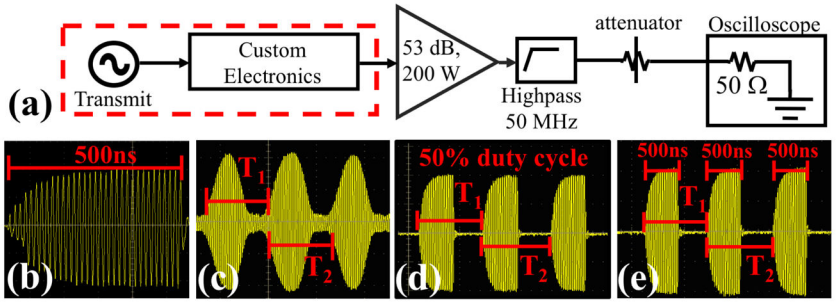

Fig. 2.

Transmit waveforms for different TAUS acquisition methods. (a) Setup used to measure transmit waveforms. The contents of the dashed red box differ for each method and are detailed in Appendix A (available in the supplementary files / multimedia tab). (b) Pulsed transmit (c) FMCW amplitude modulation (d) FMCW square-wave modulation with 50% duty cycle (e) FMCW square-wave modulation with 500 ns pulse time. In parts (c), (d), and (e), T_1 and T_2 represent the periods of consecutive cycles of the LFM chirp.

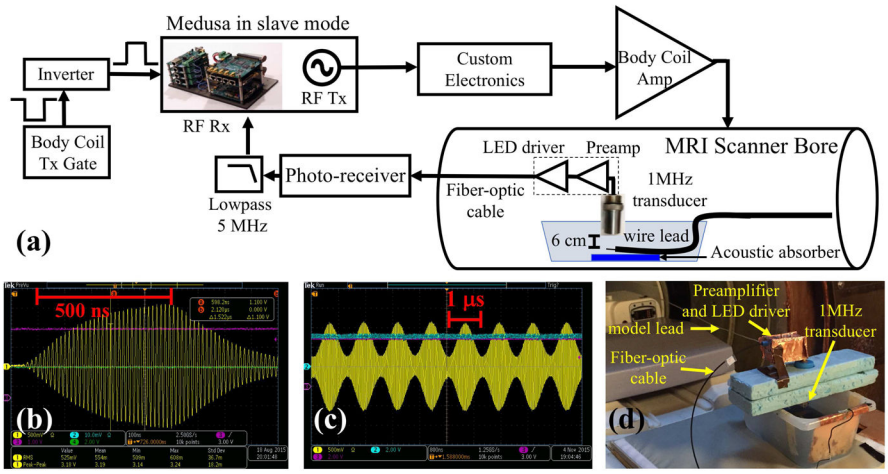

Fig. 3.

(a) Interface between TAUS system and MRI scanner allowing transmit of desired waveforms to the body coil and reception of acoustic signal. (b) Pulsed transmit signal received by pickup loop in the scanner bore, with significant rise and fall times of the signal's envelope relative to Fig. 2b due to the high-Q MRI body coil. (c) FMCW amplitude modulation transmit signal received by pickup loop in the scanner bore, with a lower modulation index than the FMCW AM signal in Fig. 2c due to filtering of the AM sidebands by the body coil. (d) Setup of lead and receive chain placed in the scanner bore

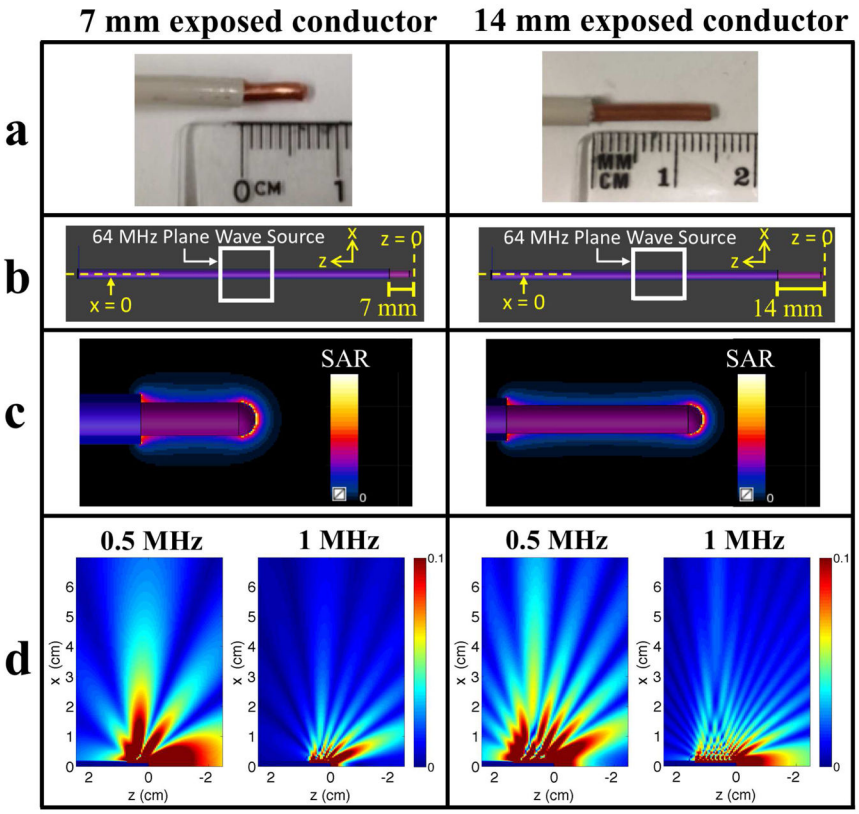

Fig. 4.

FDTD simulations of TAUS near lead tips. (a) Lead tips used as models for simulations and for experimental validation. (b) Electromagnetic simulation models in Sim4Life. Each coordinate system is defined so that the axis of rotational symmetry for each cylindrically symmetric lead is the intersection of the planes $x = 0$ and $y = 0$. The white boxes show the locations of the 64 MHz plane wave sources placed to generate electric fields oriented tangentially to the leads. (c) Simulated SAR profiles at the lead tips in the plane $y = 0$. The SAR profiles are cylindrically symmetric around the leads. (d) Relative thermo-acoustic signal magnitudes for 0.5 MHz and 1 MHz acoustic frequencies in the plane $y = 0$, displayed with 10× windowing. Negative x values are omitted due to the cylindrical symmetry around the center of the lead.

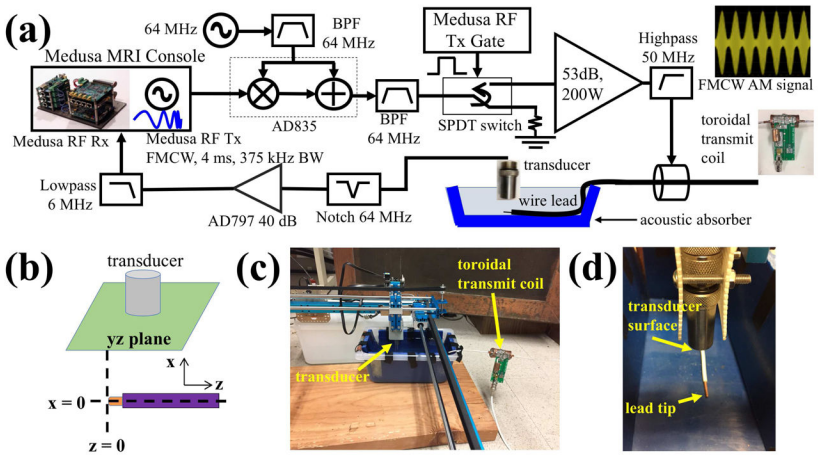

Fig. 5.

Setup used to validate TAUS simulations by performing TAUS acquisitions at different transducer positions within a plane to assess how transducer positioning relative to the lead tip affects the signal level. a) Transmit and receive chains for TAUS acquisition. b) Depiction of measurement plane (the yz plane) orientation relative to lead geometry. c) Interface between transmit coil, lead, transducer, and 2D CNC plotter. The transducer was attached to the stage of the plotter to allow for precise movement in the measurement plane. d) Position of lead tip and transducer surface in tub shown without saline solution.

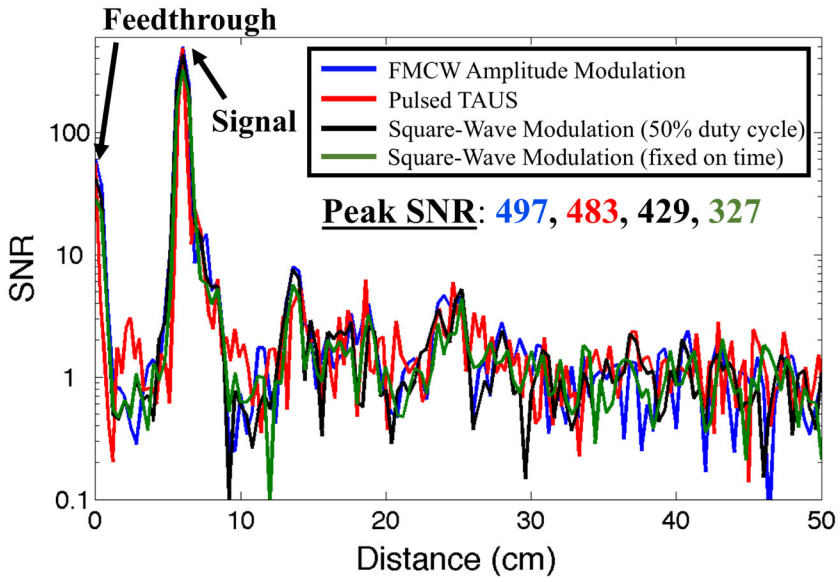

Fig. 6.

Thermo-acoustic signal when driving the stripped coaxial cable source using the same transmit power, transmit duration, and transducer positioning for the different acquisition methods. The signal peak at the 6 cm from the transducer indicates thermo-acoustic signal detection, whereas the peak at 0 distance is caused by direct feedthrough from the transmit to the receive chain.

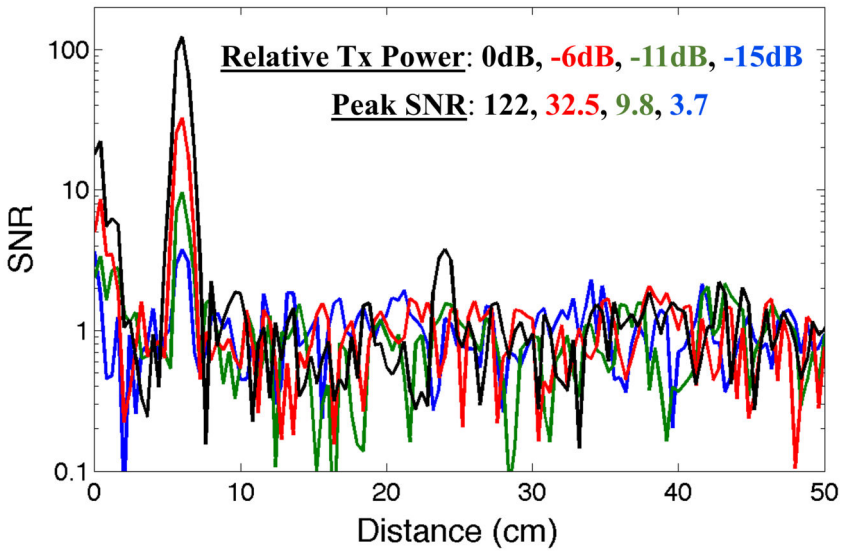

Fig. 7.

Thermo-acoustic signal detected near the tip of the model lead in the scanner bore when driving the body coil at varying transmit powers with the same transmit duration and transducer positioning. The signal peak is present at the distance between the lead tip and the transducer, and the SNR scales approximately linearly with transmit power.

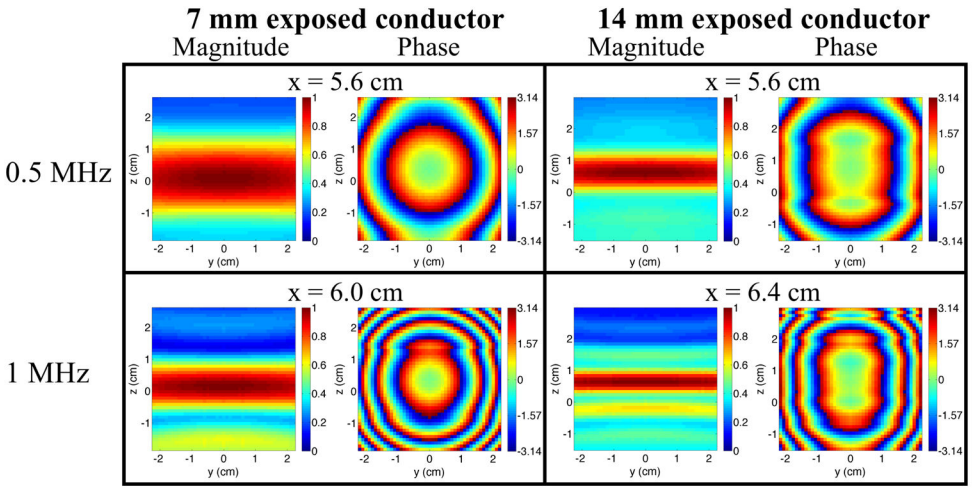

Fig. 8.

Signal profiles from FDTD simulations in a measurement plane (defined by a value of x for the coordinate system in Fig. 5b) for both leads at center frequencies of 0.5 MHz and 1 MHz. The magnitude signal is summed over a 375 kHz bandwidth, and the phase is taken at the center frequency.

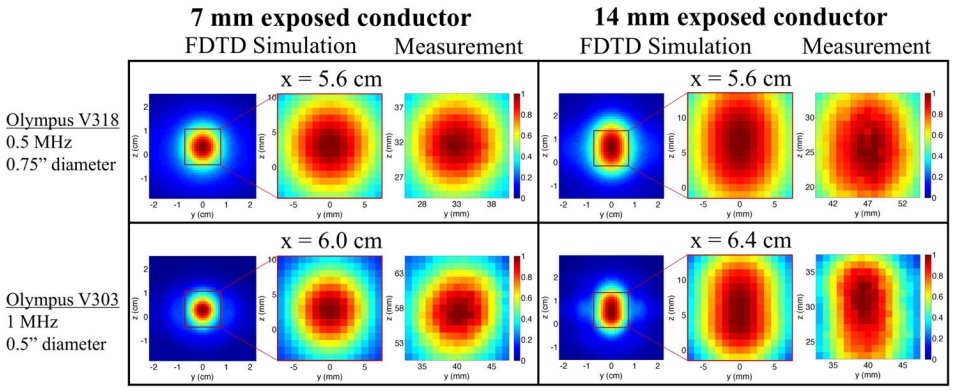

Fig. 9.

Magnitude signals for a transducer centered at various positions in a measurement plane (defined by a value of x for the coordinate system in Fig. 5b) for both leads at center frequencies of 0.5 MHz (transducer diameter of 0.75 inches) and 1 MHz (transducer diameter of 0.5 inches) obtained through measurement or FDTD simulation. The simulated signal is shown both in a 45 mm by 45 mm area of the measurement plane and in the 15 mm by 15 mm region that best matches the measured spatial pattern. The axis values for the measured data have an arbitrary offset due to the lack of registration to the lead tip.